Scaling of LWFA for Multi-PW Laser-Plasma Interaction

S. V. Bulanov, G. M. Grittani, P. Valenta

LAMU-2025
ELI-ERIC, ELI-Beamlines
March 19, 2025

Tajima, T., and Dawson, J. M., (1979), Laser electron accelerator, Phys. Rev. Lett. 43, 267

Mourou, G., Tajima, T., and Bulanov, S.V., (2006), Optics in the relativistic regime, Rev. Mod. Phys. 78, 309

Lu, W., Tzoufras, M., Joshi, C., Tsung, F. S., Mori, W. B., Vieira, J., Fonseca, R. A., and Silva, L. O., (2007), Generating multi-gev electron bunches using single stage laser wakefield acceleration in a 3d nonlinear regime. Phys. Rev. ST Accel. Beams 10, 061301

Tzoufras, M., Lu, W., Tsung, F. S., et al., (2008), Beam loading in the nonlinear regime of plasma-based acceleration. Phys. Rev. Lett. 101, 145002.

Bulanov, S. V., T. Zh. Esirkepov, Y. Hayashi, H. Kiriyama, J. K. Koga, H. Kotaki, M. Mori, and M. Kando, (2016), On some theoretical problems of laser wake-field accelerators, J. Plasma Phys. 82, 905820308

Valenta, P., Esirkepov, T. Z., Ludwig, J. D., Wilks, S. C., Bulanov, S. V., (2025), Bayesian optimization of electron energy from laser wakefield accelerator, arXiv preprint arXiv:2501.06069

Laser-Based 100 GeV Electron Acceleration Scheme for Muon Production

*J. D. Ludwig,[1] S. C. Wilks,[1] A. J. Kemp,[1] G. J. Williams,[1] N. Lemos,[1] E. Rockafellow,[2] B. Miao,[2] J. E. Shrock,[2] H. M. Milchberg,[2] J.-L. Vay,[3] A. Huebl,[3] R, Lehe,[3] A. Cimmino,[4] R. Versaci,[4] S. V. Bulanov,[4] P. Valenta,[4] V. Tang,[1] and B. A. Reagan[1]

[1)]*Lawrence Livermore National Laboratory, 7000 East Avenue, Livermore, California 94551, USA*

[2)]*Institute for Research in Electronics and Applied Physics and Department of Physics, University of Maryland, College Park, Maryland 20742, USA*

[3)]*Lawrence Berkeley National Laboratory, 1 Cyclotron Road, Berkeley, California 94720, USA*

[4)]*ELI Beamlines Facility, The Extreme Light Infrastructure ERIC, Za Radnicí 835, 252 41 Dolní Břežany, Czech Republic*

(*Electronic mail: ludwig8@llnl.gov)

(Dated: 13 November 2024)

High energy muons, due to their unique ability to penetrate deeply into matter, can enable radiography of structures that cannot be probed by other forms of radiation. Current terrestrial sources of muons require conventional GeV-TeV particle accelerators which are hundreds to thousands of meters in size. Laser wakefield acceleration (LWFA) can achieve acceleration gradients of two-to-three orders of magnitude greater than conventional accelerators, thus shrinking the accelerator to a number of meters. We propose a concept for a compact muon source based on the first self-consistent PIC simulations of an all optical LWFA that uses a guiding channel to achieve electron energies of 100 GeV in a distance of 6 meters with a driving laser energy of 300 J in a single stage. From the resulting electron energy spectrum we estimate muon production for this source. We show that this accelerator, coupled with high average power laser driver technology, provides the basis for a high energy and high flux muon source.

Muons were discovered in CR by by C. D. Anderson and S. Neddermeyer (1936)

Muon - Heavy Electron

$m_\mu = 105.66\ \mathrm{MeV}/c^2$

$m_\mu \approx 206.768\, m_e$

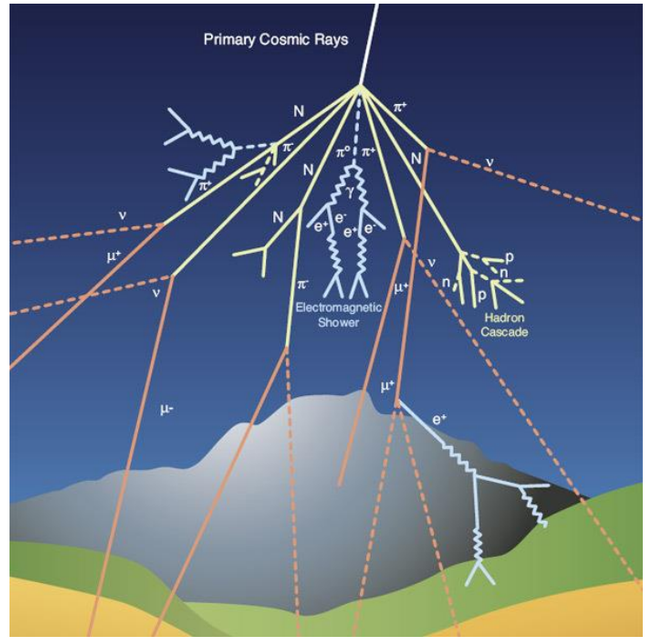

Muon decays as

$\mu^- \to e^- + \bar{\nu}_e + \nu_\mu$

$\mu^+ \to e^+ + \nu_e + \bar{\nu}_\mu$

$\tau = \hbar/\Gamma \approx 2.196\mu s \approx 2.2\times10^{-6}$.

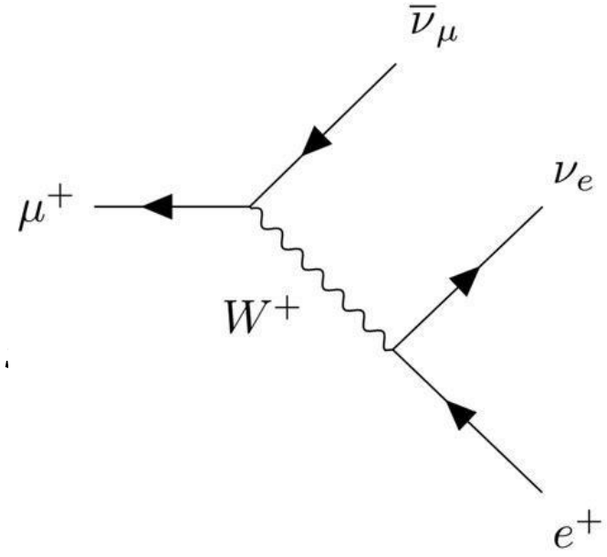

Tau lepton

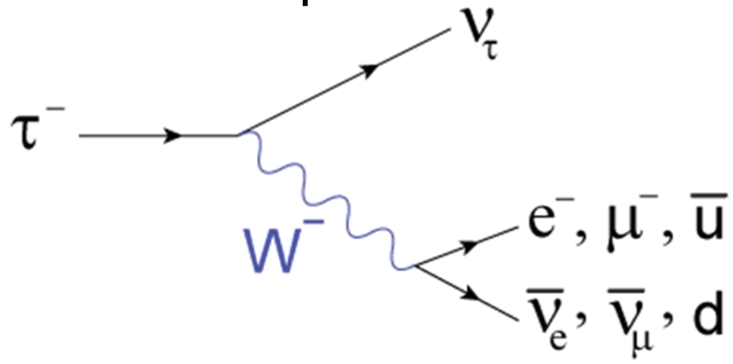

Muon creation

Pair creation via Bethe-Heitler process

$$\sigma_{e^\pm} = \alpha r_e^2 Z^2 \left[\frac{28}{9} \ln \frac{183}{Z^{1/3}} - \frac{2}{27} \right] \qquad \sigma_{\mu^\pm} = \sigma_{e^\pm} \left(\frac{m_e}{m_\mu} \right)^2 \approx \frac{\sigma_{e^\pm}}{40000}$$

$$\alpha = \frac{e^2}{\hbar c} \approx \frac{1}{137} \quad \Rightarrow$$

$$r_e = \frac{e^2}{m_e c^2} \approx 2.8 \times 10^{-13}\,\text{cm} \qquad r_\mu = \frac{e^2}{m_\mu c^2} \approx 2.8 \times 10^{-13}\,\text{cm}$$

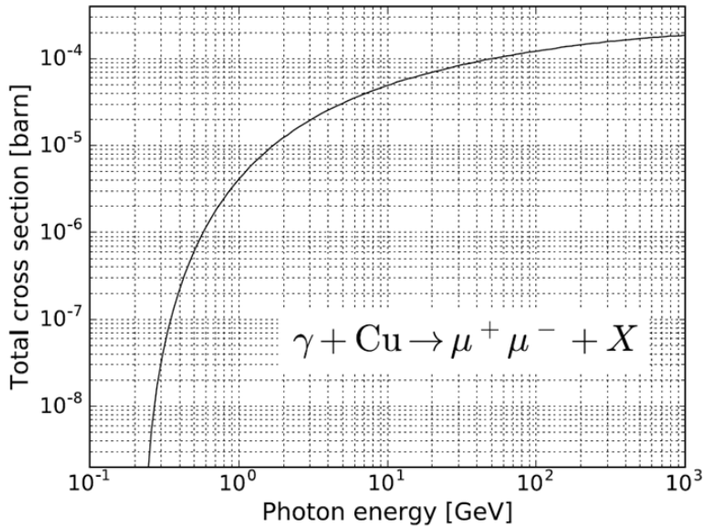

Fig. 3. An incident photon energy dependence of the total cross section for the muon pair production on a copper target.

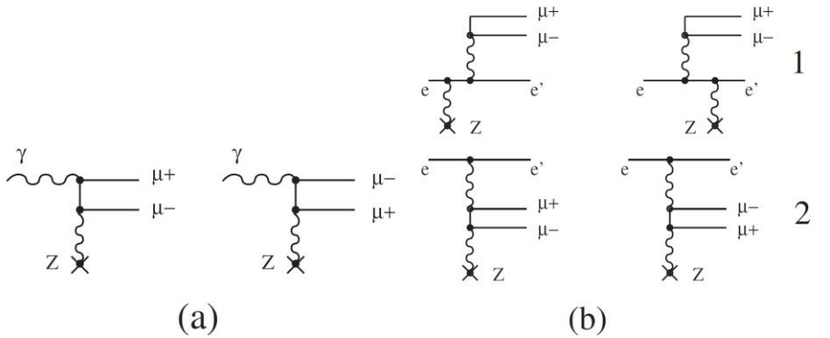

FIG. 1. Diagrammatic representation of dimuon production processes in electromagnetic interactions. (a) Bethe-Heitler process $\gamma + A \to A + \mu^+\mu^-$. (b) Electron induced reaction $e + A \to e + A + \mu^+\mu^-$.

High energy muon beam generation (ICMuS2 project)

DARPA's Muons for Science & Security program aims to create a compact source of deeply penetrating subatomic particles known as muons to enable a variety of scientific, commercial, and defense applications – from medical diagnostics, to scans of cargo containers for dangerous materials. MuS2 project aims to employ laser plasma acceleration to develop scalable and practical processes to produce conditions that can create muons exceeding 100 GeV. This unique muon source will also be available for multidisciplinary experiments including the astrobiology.

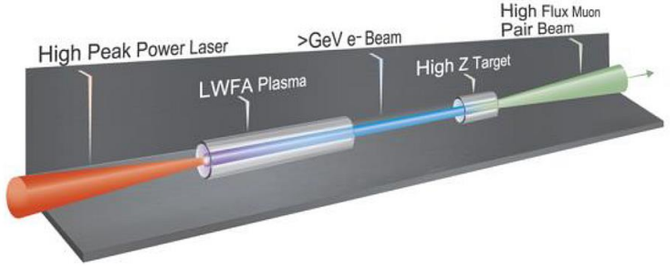

L4-Aton laser at ELI-Beamlines has optimized parameters for LWFA: 1.5 kJ, 150 fs, 100s shots/day.
10 PW electron acceleration set-up being designed to enable experiments in the near future

MUON TOMOOGRAPHY: 10 PW electron acceleration as a driver for muon production

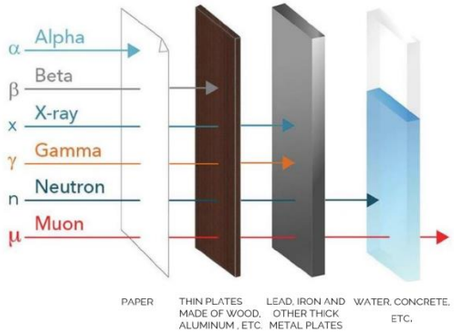

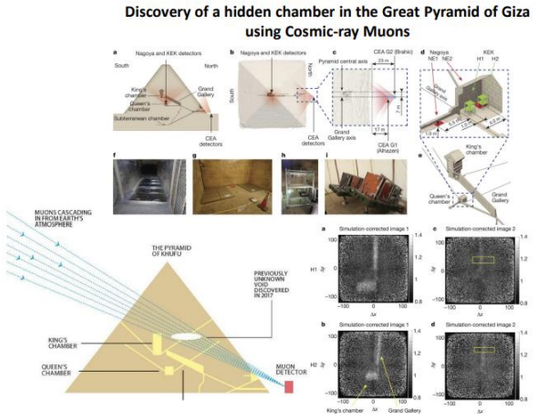

Archeology

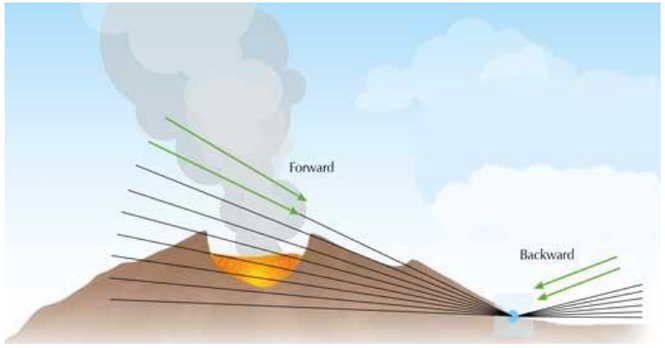

Volcanology

Fukushima tomography

Laser Wake Field Acceleration

I.
a) Wake field generated by short laser pulse
b) Relativistic Langmuir wave
c) Optimal length of the driver pulse
d) The LWFA energy scaling
e) Relativistic self-focusing
f) Basic mechanisms of the electron injection

II.
a) High-energy muon beam production
e) Medical applications
f) Compact XFEL

Relativistically strong laser pulse interaction with underdense plasma

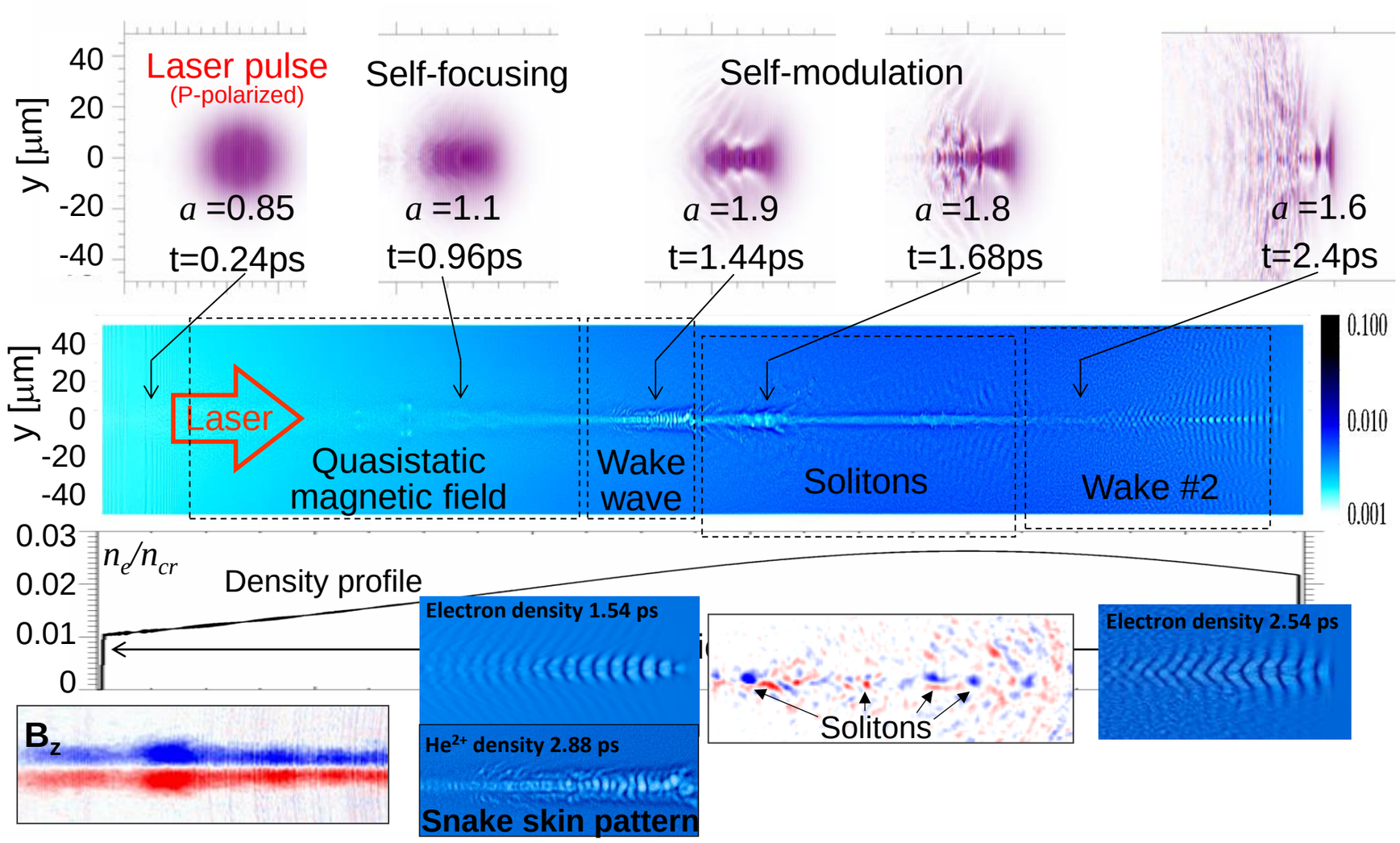

(2007)

Wakefield Generated by Short Laser Pulse (Tajima&Dawson 1979)

Wake Plasma Wave

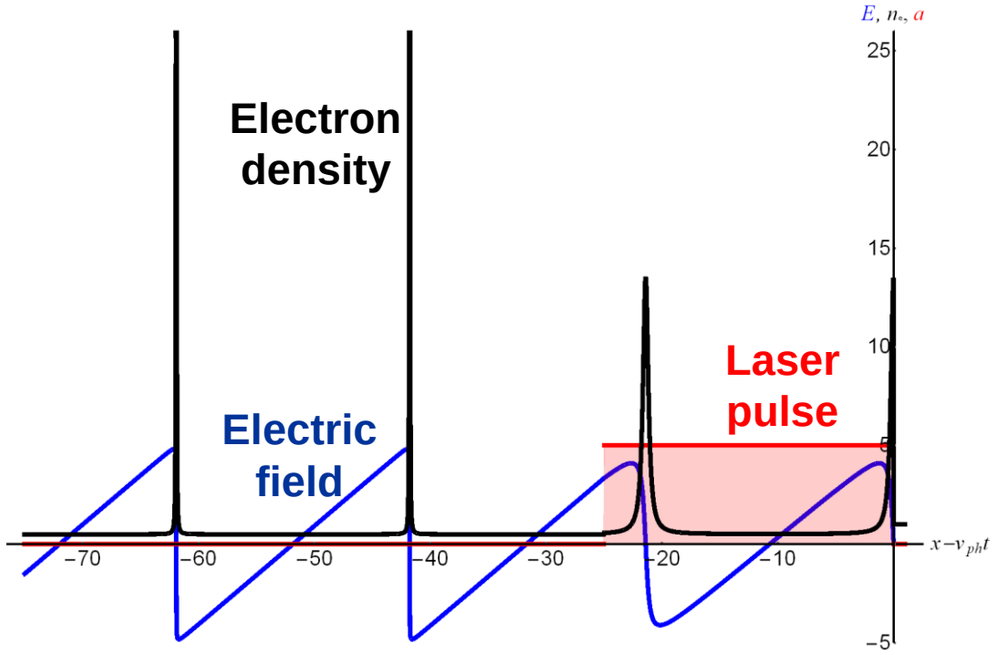

$$\lambda_w = 2\pi / k_w, \quad k_w v_{ph} = \omega_w, \quad \gamma_{ph} = 1/\sqrt{1 - v_{ph}^2 / c^2}$$

$$\omega_w = \omega_{pe} \begin{cases} 1 - 3(p_m / m_e c)^2 / 16, & p_m / m_e c \ll 1 \\ \pi / \sqrt{2 p_m / m_e c}, & p_m / m_e c \gg 1 \end{cases}$$

$$\omega_{pe} = \sqrt{4\pi n e^2 / m_e}$$

Wakewave Breaking Threshold

$$E_{A-P} = (m_e \omega_{pe} c / e)\sqrt{2(\gamma_{ph} - 1)}$$

Limit $\beta_w \to 1$; Optimal Length of the Driver Pulse

Electrostatic potential obeys

$$\varphi'' = \frac{1}{2}\left(\frac{1+a^2}{(1+\varphi)^2} - 1\right), \text{ where } \gamma_w = 1/\sqrt{1-\beta_w^2}$$

Maximum electric field in the wave $|E_m| = \sqrt{1+a^2} - 1$

Optimal length of the laser pulse

$$l_{opt} = \int_0^{a^2} \sqrt{\frac{1+\varphi}{\varphi(a^2-\varphi)}}\, d\varphi = 2E(-a^2)$$

here $E(k)$ is the complete elliptic integral of the 2nd kind.

In the limit $|a| << 1$

$$l_{opt} = \pi + \frac{\pi}{4}a^2 - \frac{3\pi}{64}a^4 + O[a^2]^3$$

For $|a| >> 1$

$$l_{opt} = 2|a| + \left(\frac{1}{2} + 2\ln 2 - \ln|a|\right)\frac{1}{|a|} + O\left[\frac{1}{|a|}\right]^3$$

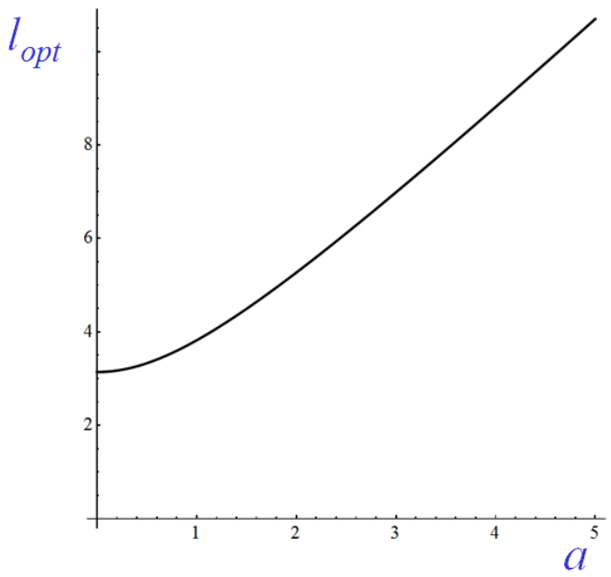

Optimal laser length vs pulse amplitude

Electrostatic potential varies in the wake

behind the pulse $$-\frac{a^2}{1+a^2} < \varphi < a^2$$

Maximum electric field in the wake

$$|E_m| = \frac{a^2}{\sqrt{1+a^2}}$$

On the LWFA energy scaling

Scaling of LWFA accelerated electrons $\mathcal{E}_e = m_e c^2 \gamma_{ph}^2 a^3$,

where $\gamma_{ph} = \frac{\omega_0}{\omega_{pe}} = \left(\frac{n_{cr}}{n}\right)^{1/2}$ and $a = \frac{eE_0}{m_e \omega_0 c}$

Energy scaling $\mathcal{E}_e = 2m_e c^2 \gamma_{ph}^2 a^2$; the acceleration length $l_{acc} = \lambda_0 a^{3/2} \gamma_{ph}^3$

with the laser amplitude $a = \left(\frac{\mathcal{P}}{\bar{\mathcal{P}}} \gamma_{ph}^{-2}\right)^{1/3}$

Electron energy depends on the laser power $\mathcal{P}$ and

on the plasma density via γ_{ph} as $\mathcal{E}_e = 2m_e c^2 \left(\frac{\mathcal{P}}{\bar{\mathcal{P}}} \gamma_{ph}\right)^{2/3}$

As a result of the laser pulse self - focusing at the threshold we have

$\mathcal{P} = \bar{\mathcal{P}} \gamma_{ph}^2$ with the laser power $\mathcal{P}$ and $\bar{\mathcal{P}} = 2m_e^2 c^5 / e^2 = 17\text{GW}$

For the e.m. field inside the s.f. channel of radius $r_w = c a^{1/2} / \omega_{pe}$

these yield for the laser amplitude $a = \left(\frac{\mathcal{P}}{\bar{\mathcal{P}}} \gamma_{ph}^{-2}\right)^{1/3}$

What is the focal length? $l_{foc} \approx \pi w_B w_0 / \lambda_0 \approx 60\text{m}$

On the LWFA energy scaling: at the self-focusing threshold

At the self - focusing threshold we have $a_0 \approx 1$

It gives the accelerated electron energy

$$\mathcal{E}_e = m_e c^2 \frac{\mathcal{P}}{\bar{\mathcal{P}}} :$$

for $\mathcal{P} = 10PW$ electron energy is 100 GeV

since $\gamma_e = \frac{\mathcal{E}_e}{m_e c^2} = 2 \times 10^5 = \gamma_{ph}^2$

we find $\gamma_{ph} = 450$

(plasma density = 2×10^{16} cm^{-3}

&

the s - f threshold is $\mathcal{P} < 8.5$ PW)

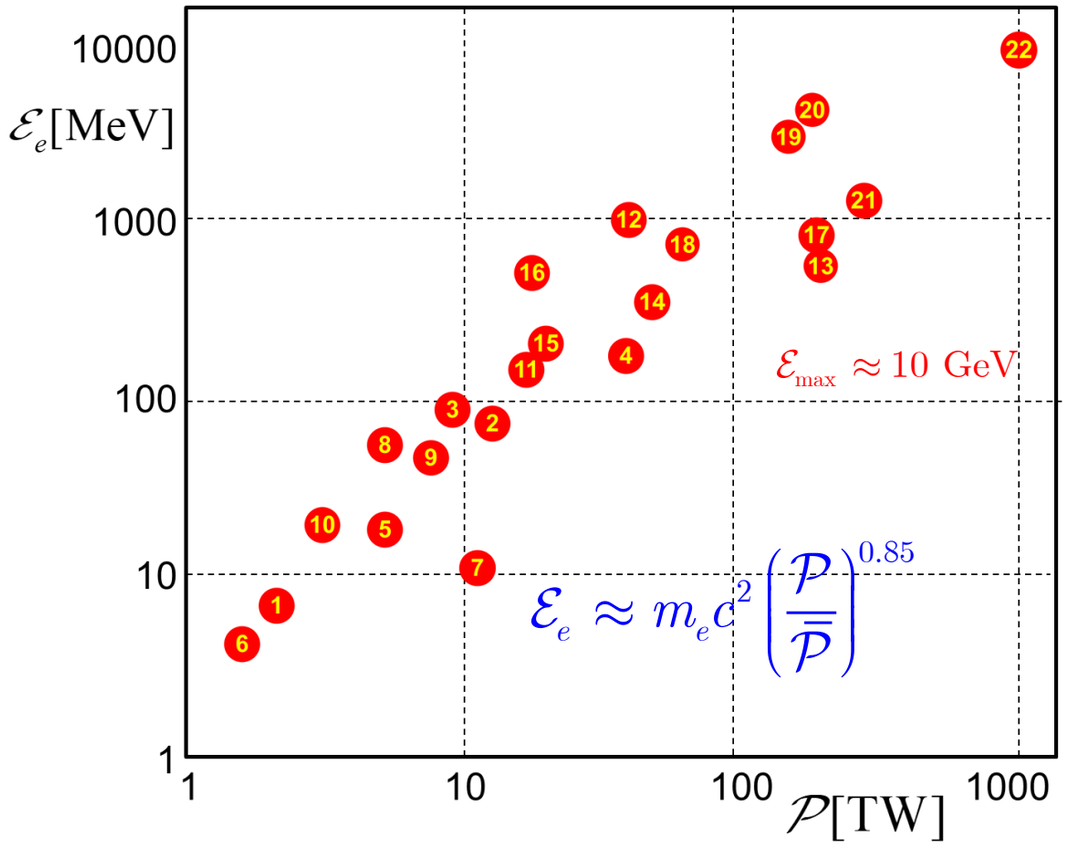

Experimental results :

LWFA electron energy vs laser power

SVB et al., J. Plasma Phys. 82, 905820308 (2016)

Electron Trapping into Wake Wave

Wake wave wavelength

$$\lambda_w = \lambda_0 \frac{\sqrt{\gamma_w} E(-a^2)}{\pi}$$

The electron acceleration length

$$l_{acc} \approx \frac{\lambda_w}{4(1-\beta_w)}$$

i.e. $(\gamma_e = 2\gamma_w^2)$

$$l_{acc} \approx \lambda_0 \gamma_w^3 \quad \text{or} \quad l_{acc} \approx \lambda_0 \gamma_e^{3/2}$$

From the analysis of the Hamiltonian

$$\mathcal{H} = \sqrt{1 + (p_\perp - a(x,t))^2 + p_\parallel^2} - \varphi(x,t)$$

with $\varphi_{\min} = -a^2/(1+a^2)$ and $\varphi_{\max} = a^2$

we obtain the threshold of the injection energy

$$\gamma_{inj} = \sqrt{1+a^2}\gamma_w \text{ i.e. } \beta_{inj} = \beta_w$$

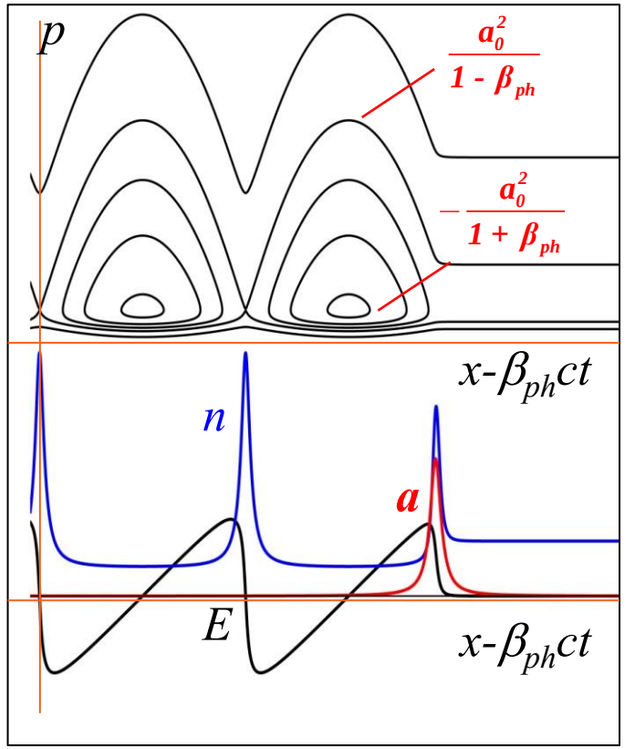

$$\sqrt{m_e^2 c^4 + p^2 c^2} - \beta_{ph} cp - e\varphi(X) = \text{constant}$$

Transverse Wake Wave Breaking

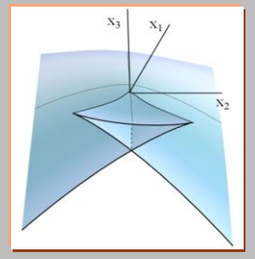

Swallow-tail singularity in local coordinates:

$$y^4 + x_1 y^2 + x_2 y + x_3 = 0$$

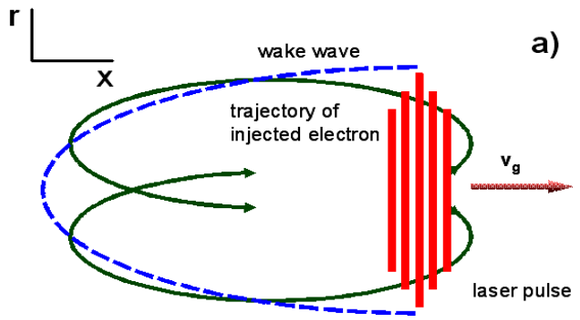

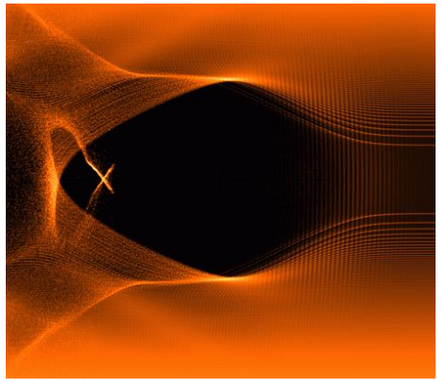

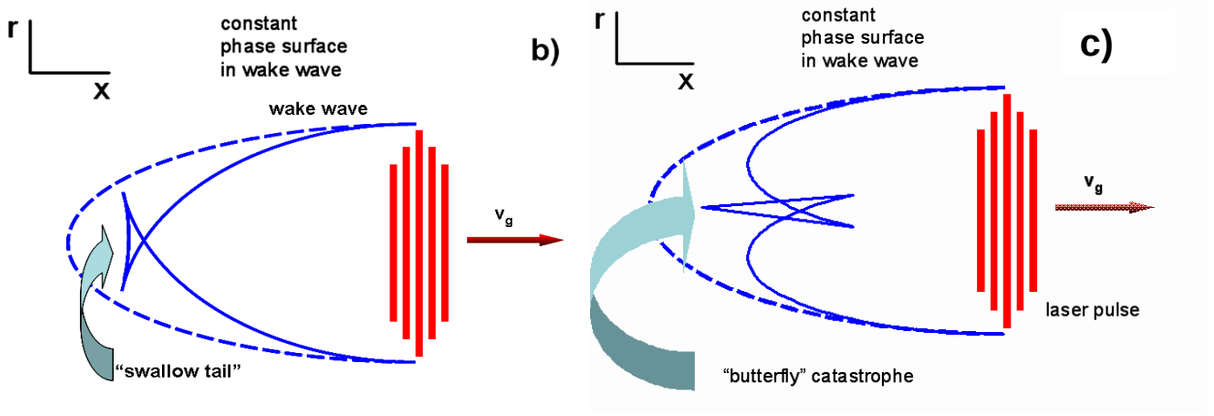

BULANOV, S. V., PEGORARO, F., PUKHOV, A. M., SAKHAROV, A.,Transverse-wake wave breaking. *Phys. Rev. Lett.* **78**, 42054208 (1997)

Down-ramp (as well as up-ramp) density injection

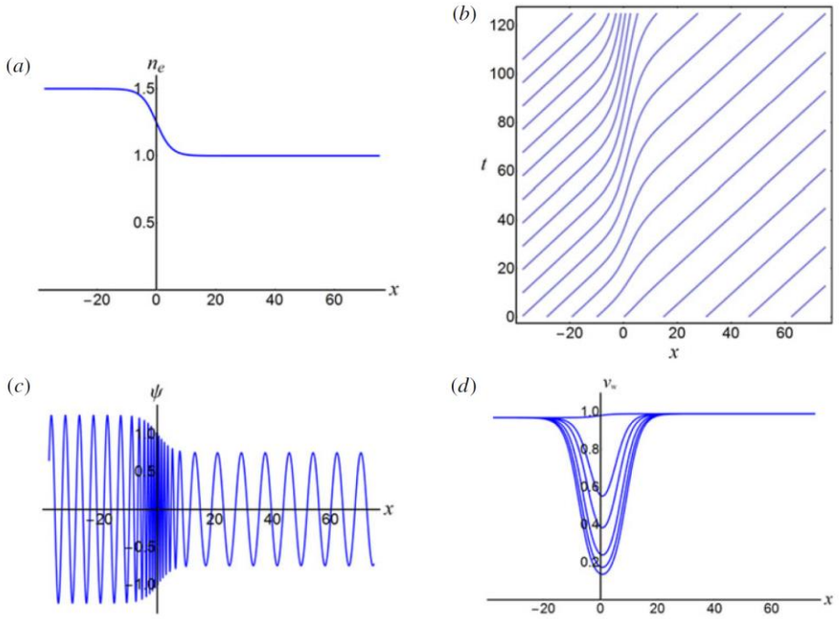

FIGURE 6. Plasma inhomogeneity effects on the phase velocity of the wake wave. (*a*) Electron density profile given by (3.21) with $n_1 = 1.5$, $n_2 = 1$, and $L = 5$. (*b*) The trajectories of the constant phase points in the (x, t) plane. (*c*) The phase dependence on the coordinate x at $t = t_m$ for $t_m = 125$. (*d*) The wake wave phase velocity v_{ph} versus coordinate x at $t = 0$, $0.125t_m$, $0.25t_m$, $0.5t_m$, $0.75t_m$, t_m. Plots are drawn in arbitrary units.

$$\partial_t k = -\partial_x \omega$$

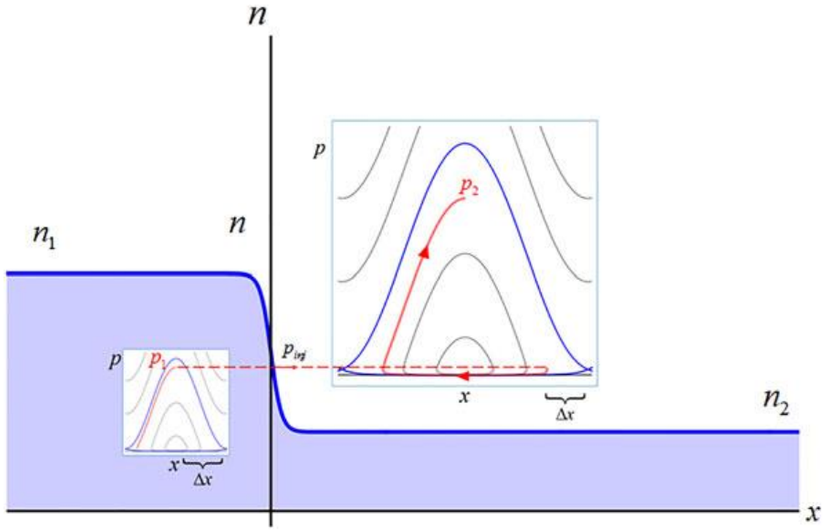

S. V. Bulanov, N. M. Naumova, F. Pegoraro, and J.-I. Sakai, "Particle Injection into the Acceleration Phase of the Wake Field behind the Laser Pulse", *Phys. Rev. E* **58**, 5257 (1998)

Cluster-plasma (nano-particle) injection

Y. Fukuda, Y. Akahane, M. Aoyama, Y. Hayashi, T. Homma, N. Inoue, M. Kando, S. Kanazawa, H. Kiriyama, S. Kondo, H. Kotaki, S. Masuda, M. Mori, A. Yamazaki, K. Yamakawa, E. Yu. Echkina, I. N. Inovenkov, J. Koga, and S. V. Bulanov, "Ultrarelativistic electron generation during the intense, ultrashort laser pulse interaction with clusters", *Physics Letters A* **363**, 130 (2007).

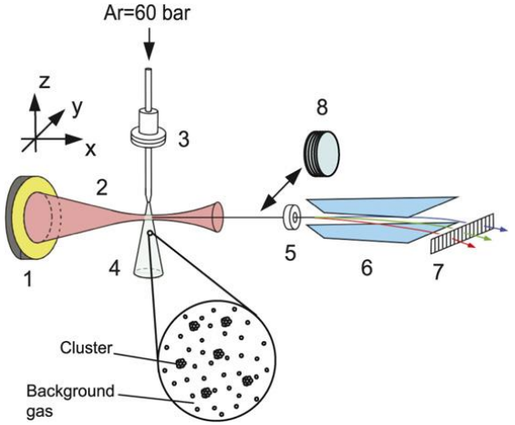

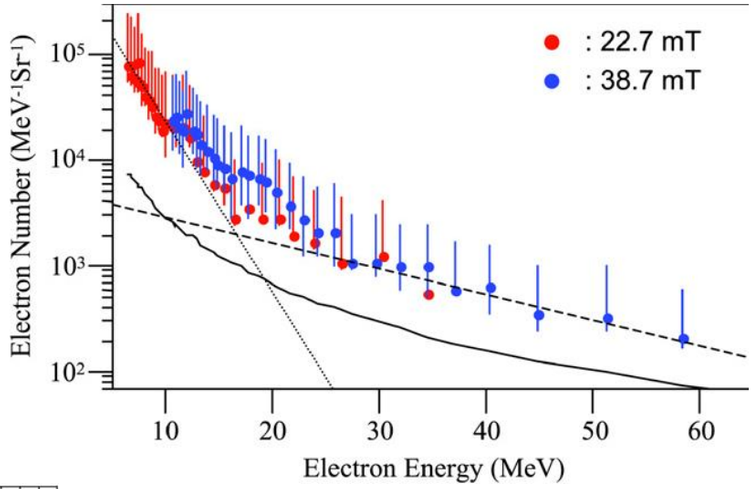

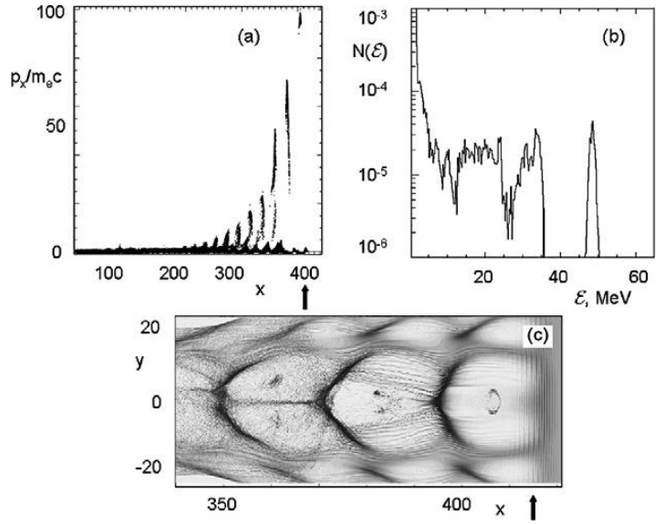

M. W. Mayr, B. Spiers, R. Aboushelbaya, R. W. Paddock, J. D. Sadler, C. Sillett, R. H. W. Wang, K. Krushelnick, and P. A. Norreys, "Nonlinear wakefields and electron injection in cluster plasma", Phys. Rev. Accel. Beams **23**, 093501 (2020)

Cho, Myung Hoon; Pathak, Vishwa Bandhu; Kim, Hyung Taek; Nam, Chang Hee, "Controlled electron injection facilitated by nanoparticles for laser wakefield acceleration", Sci. Rep. **8**, 19264 (2018)

Optical Injection

D. Umstadter J. K. Kim, and E. Dodd, *Phys. Rev. Lett*. **76,** 2073 (1996); E. S. Dodd, J. K. Kim, and D. Umstadter, *Phys. Rev. E* **70,** 056410 (2004); E. Esarey et al., *Phys. Rev. Lett*. **79**, 2682 (1997); C. B. Schroeder et al., *Phys. Rev. E* **59**, 6037 (1999); E. Esarey et al., Phys. Plasmas 6, 2262 (1999). J. Faure et al., Nature (London) 444, 737 (2006). H. Kotaki, I. Daito, M. Kando, Y. Hayashi, K. Kawase, T. Kameshima, Y. Fukuda, T. Homma, J. Ma, L.-M. Chen, T. Zh. Esirkepov, A. S. Pirozhkov, J. K. Koga, A. Faenov, T. Pikuz, H. Kiriyama, H. Okada, T. Shimomura, Y. Nakai, M. Tanoue, H. Sasao, D. Wakai, H. Matsuura, S. Kondo, S. Kanazawa, A. Sugiyama, H. Daido, and S.V. Bulanov, "Electron Optical Injection with Head-On and Countercrossing Colliding Laser Pulses", *Phys. Rev. Lett.* **103,** 194803 (2009).

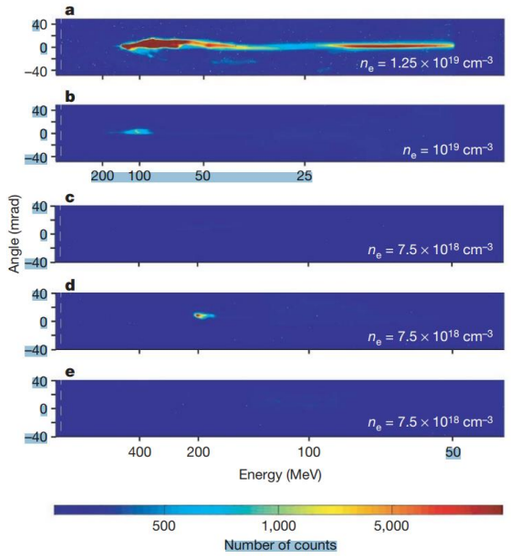

Figure 1 | Raw images of the electron beam obtained with the electron spectrometer. Horizontal axis, electron energy; vertical axis, angular divergence. The colour scale reflects the number of counts which gives an indication of the beam charge. **a**–**c** were obtained with the pump laser pulse only. **a**, The image shows an intense self-injected electron beam with a broad energy distribution ($n_e = 1.25 \times 10^{19}$ cm^{-3}). In **b** the self-injected electron beam has less charge but a quasi-monoenergetic distribution ($n_e = 10^{19}$ cm^{-3}). In **c** there is no electron beam, because the density is below the threshold for self-injection ($n_e = 7.5 \times 10^{18}$ cm^{-3}). **d** was obtained by colliding the pump with the injection pulse with parallel polarizations, at the same plasma density ($n_e = 7.5 \times 10^{18}$ cm^{-3}). A high-quality monoenergetic electron beam at 200 MeV is produced. **e**, When the polarizations of the laser beams are crossed, no injection occurs.

J. Faure et al.

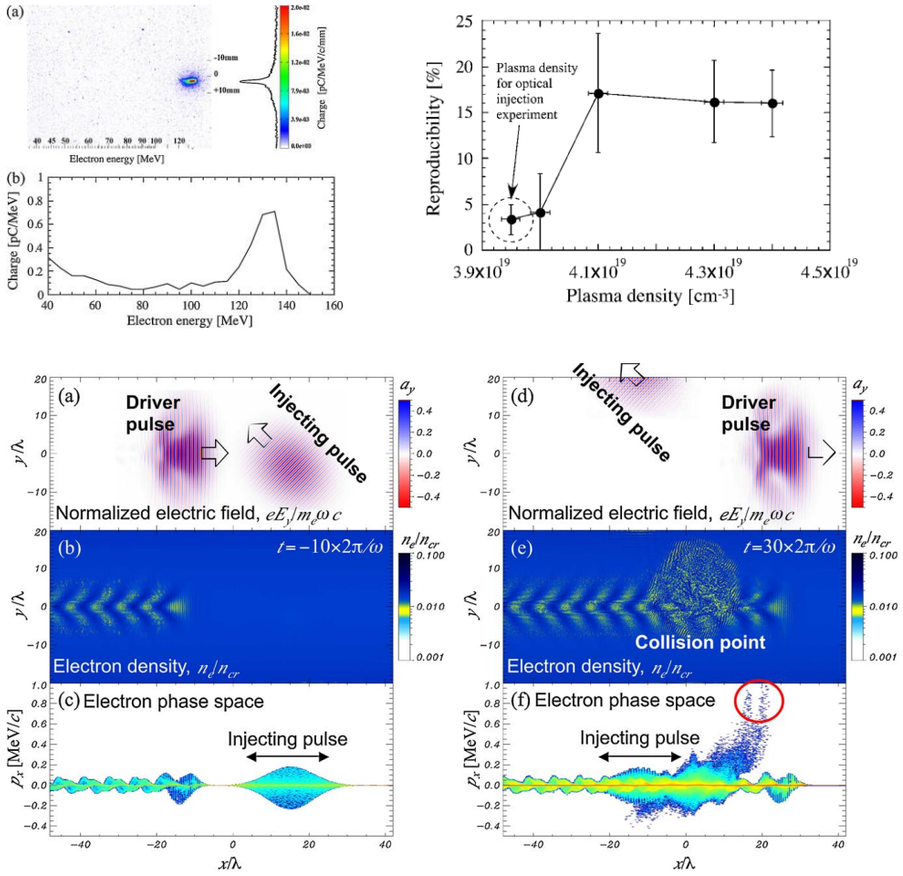

H. Kotaki et al.

Beam Loading

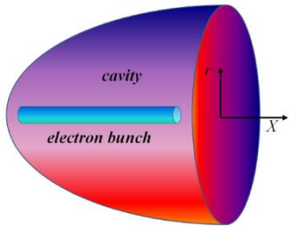

Electron bunch equilibrium inside the wake wave assuming that its transverse size is substantially less than the longitudinal one.

Equations of motion and the Maxwell equations

$$\partial_t n^b + \frac{1}{r}\partial_r (r n^b v_r^b) = 0$$

$$\partial_t p_r^b + v_r^b \partial_r p_r^b - \frac{v_\theta^b p_\theta^b}{r} = -e(E_r + \beta_x^b B_\theta)$$

$$\partial_t p_\theta^b + v_r^b \partial_r p_\theta^b - \frac{v_r^b p_\theta^b}{r} = 0$$

$$\frac{1}{r}\partial_r (r E_r^b) = 4\pi e(n^b - n_0)$$

$$\frac{1}{r}\partial_r (r B_\theta^b) = 4\pi e n^b c \beta_x^b$$

Using the Lagrange variables,

$r = r_0 + \rho(r_0, t)$ and t,

we reduce this problem to

$$\partial_{tt}\rho + \omega_b^2 (r_0 + \rho) = \frac{M_\theta^{b2}(r_0)\gamma^{b2} + 2e^2 m_e N^b(r_0)(r_0+\rho)^2}{m_e^2 \gamma^b (r_0+\rho)^3}$$

where $\omega_b^2 = \omega_{pe}^2 / 2\gamma^b$

This is similar to Kapchinskij - Vladimirskij equations.

At the equilibrium the bunch density is ($\Omega^b = M_\theta^b / r^2$)

$$n^b = n_0 \gamma^{b2} - \frac{m_e \Omega^{b2} \gamma^{b3}}{2\pi e^2}$$

This gives the overloading threshold

$$N_{tot}^b = \frac{\lambda}{6\pi r_e}\left(\frac{\mathcal{P}}{\bar{\mathcal{P}}}\right)^{1/2} \quad \text{with } r_e = \frac{e^2}{m_e c^2}$$

For 10 PW laser we have $N_{tot}^b \approx 7.5\times 10^9$

TZOUFRAS, M., LU, W., TSUNG, F. S., HUANG, C., MORI, W. B., KATSOULEAS, T., VIEIRA, J., FONSECA, R. A. & SILVA, L. O. 2008 Beam loading in the nonlinear regime of plasma-based acceleration. *Phys. Rev. Lett*. **101**, 145002.

Optimization of the LWFA Parameters for ICMuS2

- LWFA relies on efficient and continual energy transfer from driver to wakefield

- Conditions for "matched" laser and plasma parameters:

$$a_0 = 2\,(P_0/P_c)^{1/3},\;\; w_0 = 2c/\omega_p\sqrt{a_0},\;\; l_0 = l_{opt} \approx \lambda_w/2$$

where $P_c \approx 17.4\,\mathrm{GW} \times n_c/n_e$ is the critical power for relativistic self-focusing

- if $P_0/P_c \gg 1$ … laser is likely to develop filamentation instability
- if $l_0/l_{opt} \gg 1$ … laser is likely to develop self-modulation instability

preferably $P_0/P_c \approx 1$ and $l_0/l_{opt} \approx 1$

Simulation setup: 100 J case

self-modulation

filamentation

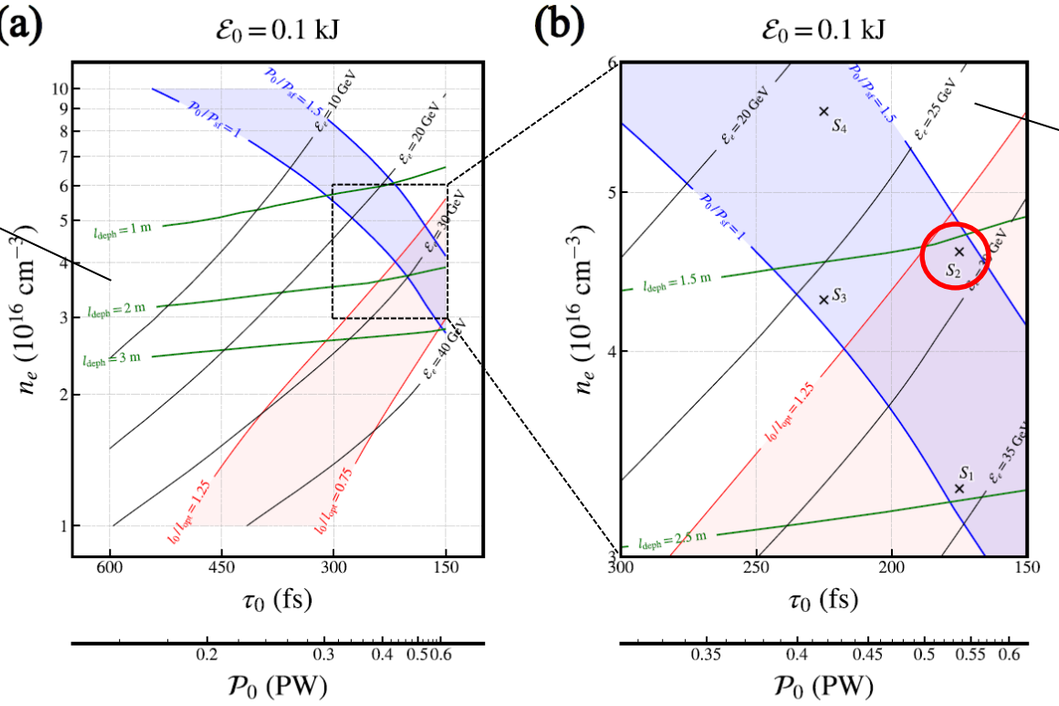

Figure 1: (a) Contours in the parameter space for $\mathcal{E}_0 = 0.1$ kJ and (b) zoom to the region of interest. Symbols S_1 and S_2 mark selected cases.

#	$\mathcal{E}_0$ (kJ)	$\mathcal{P}_0$ (PW)	τ_0 (fs)	w_0 (μm)	a_0	n_e (cm^{-3})	$\mathcal{E}_{\max}$ (GeV)	l_{acc} (m)
S_1	0.1	0.54	175	83	2.02	3.3×10^{16}	34	2.44
S_2	0.1	0.54	175	74	2.26	4.6×10^{16}	29	1.54
S_3	0.1	0.42	225	73	2.03	4.3×10^{16}	26	1.63
S_4	0.1	0.42	225	67	2.21	5.6×10^{16}	22	1.13

Table 1: Parameters of four selected cases, S_1 - S_4, for $\mathcal{E}_0 = 0.1$ kJ.

Simulation setup: 500 J case

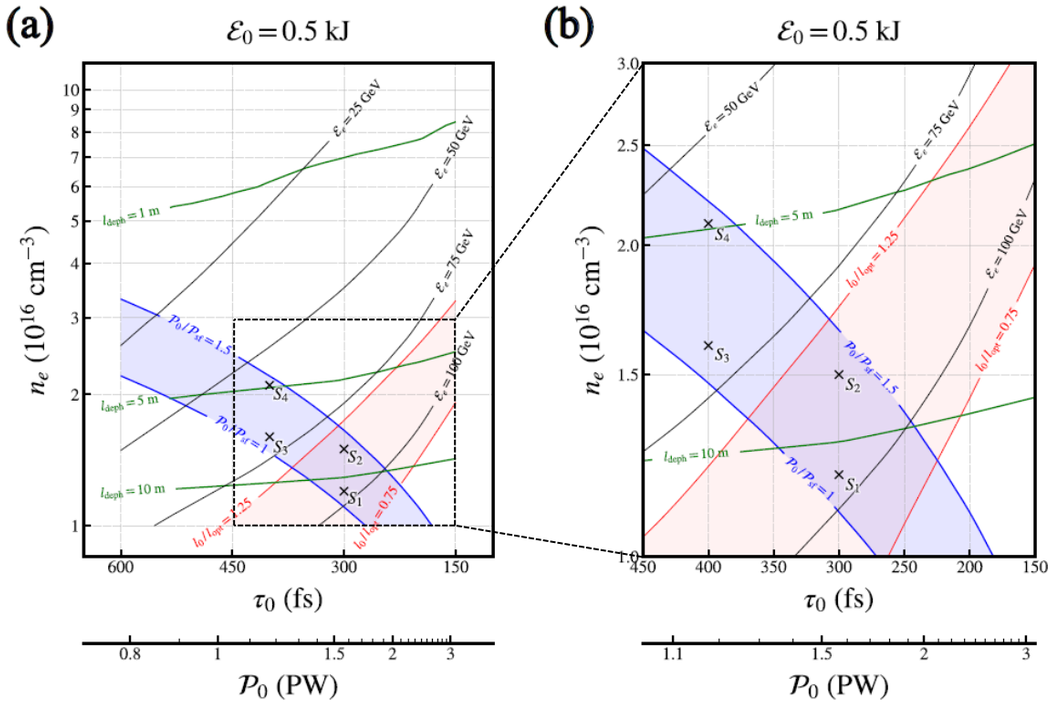

Figure 5: (a) Contours in the parameter space for $\mathcal{E}_0 = 0.5$ kJ and (b) zoom to the region of interest. Symbols S_1 and S_2 mark selected cases.

#	$\mathcal{E}_0$ (kJ)	$\mathcal{P}_0$ (PW)	τ_0 (fs)	w_0 (μm)	a_0	n_e (cm^{-3})	$\mathcal{E}_{\max}$ (GeV)	l_{acc} (m)
S_1	0.5	1.57	300	139	2.06	1.2×10^{16}	96	11.21
S_2	0.5	1.57	300	129	2.22	1.5×10^{16}	86	8.38
S_3	0.5	1.17	400	120	2.06	1.6×10^{16}	70	7.16
S_4	0.5	1.17	400	110	2.25	2.1×10^{16}	58	4.88

Table 5: Parameters of four selected cases, S_1 - S_4, for $\mathcal{E}_0 = 0.5$ kJ.

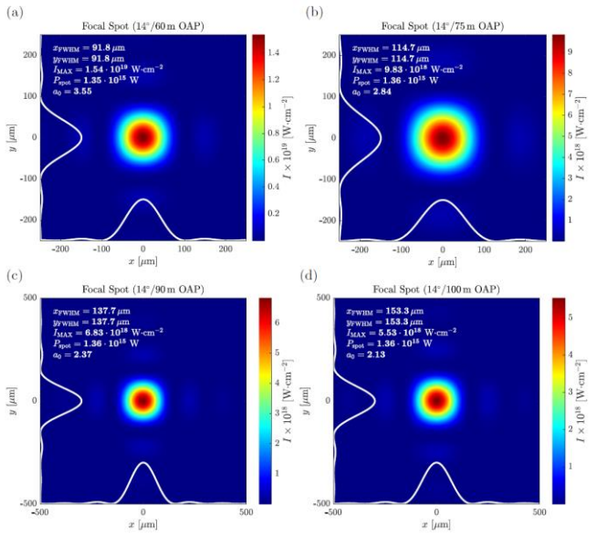

Figure 6: L4 beam of pulse energy 500 J and pulse length 300 fs focused by an ideal off-axis parabolic mirror at 14° off-axis angle for various focal lengths, (a) $f = 60$ m, (b) $f = 75$ m, (c) $f = 90$ m and (d) $f = 100$ m. The peak power is $\mathcal{P}_0 = 1.57 \cdot 10^{15}$ W.

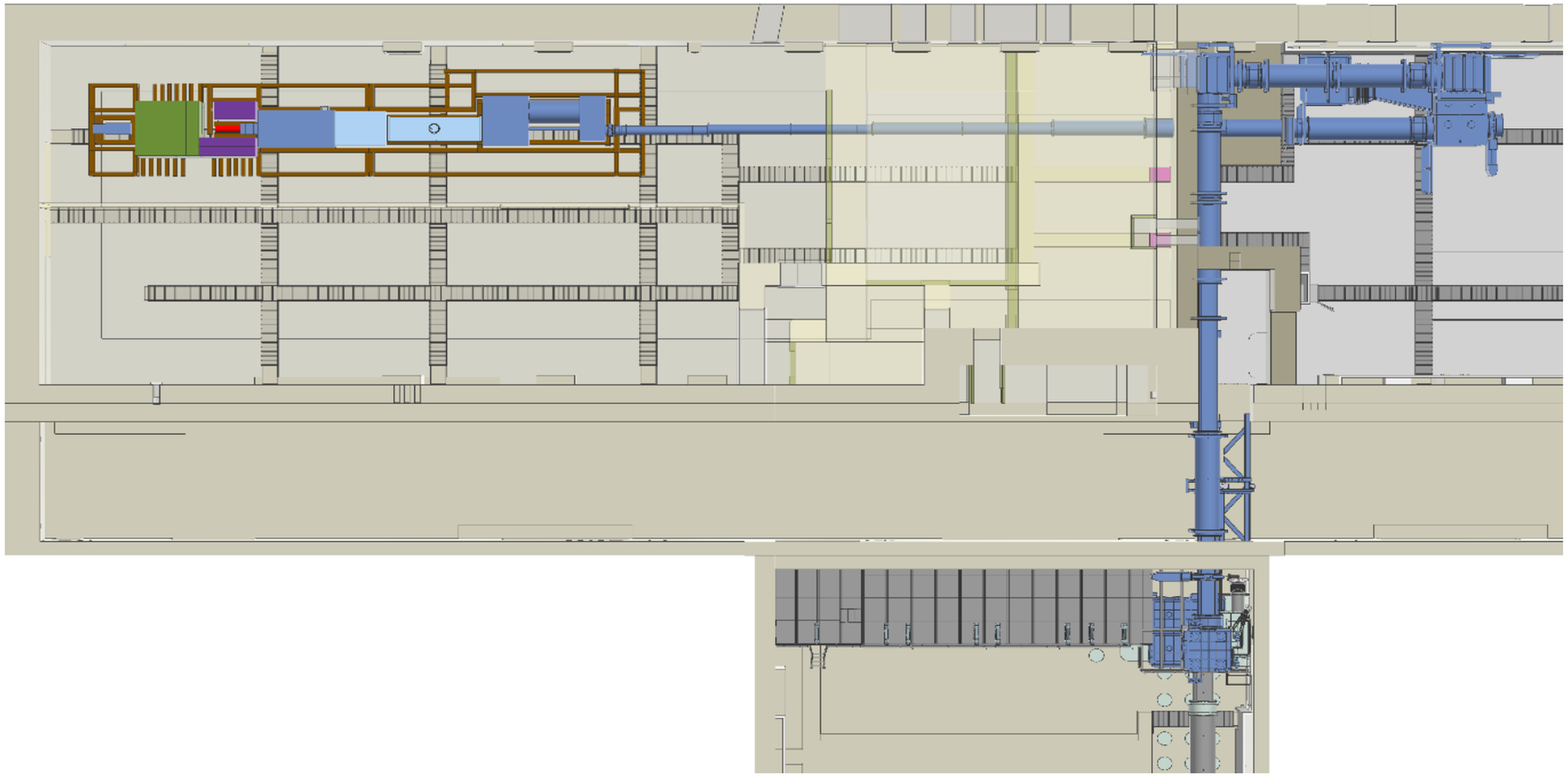

Technical Design Report (TDR)

Thank you for your attention!